Steady Uniaxial Elongational Flows: Roles of Intramolecular Potentials

Anand S. Bhandar and John M. Wiest*

Department of Chemical Engineering, University of Alabama, Tuscaloosa, Alabama 35487

Received August 2, 2000; Revised Manuscript Received June 1, 2001

ABSTRACT: We examine the roles of several types of intramolecular interactions in the behavior of the steady elongational flow properties of infinitely dilute polymer solutions. In particular, bond stretching, bond bending, bond torsion, and nonbonded intramolecular interactions are included. Geometric and rheological properties are calculated using Monte Carlo integration. We observe that bond bending and nonbonded interactions result in significant changes over the traditional bond stretching predictions, but bond torsion plays only a minor role. Bond bending results in more abrupt chain expansion with increasing elongation rate, and the corresponding increase in the elongational viscosity is also more steep. Nonbonded interactions cause the chain to be more spheroidal at lower elongation rates, and they result in a minimum in the elongational viscosity at an intermediate elongation rate—presumably as a result of excluded-volume effects causing the chain to be slightly more expanded.

Introduction

Extensional flows of dilute polymer solutions have been the subject of long-standing interest, because these flows can distort the molecules substantially and allow examination of conformational rearrangement. The relevant literature indicates an alternating and consequential series of theoretical and experimental advances. In early polymer kinetic theories, extensional flows were examined because their irrotational nature simplified calculations. These calculations spurred much experimental work, but realizing controlled extensional flows for dilute solutions has always been very difficult. A wide variety of ingenious devices were constructed to approximate such flows. These included four-roll mills,[1−3] crossed-slot or converging channel devices,[4−13] and opposing jet or nozzle devices.[14−22] All of these devices suffer from deficits in that the kinematics imposed on a fluid element are not purely extensional (they involve shearing components), and/or the flows are inherently unsteady in a Lagrangian sense (a fluid element experiences kinematics that vary with time). They have, nonetheless, provided a great deal of insight into the behavior of polymer solutions in stretching flows. They have also spawned many theoretical attempts to explain their results.[23−31]

Interest in extensional flows of dilute polymer solutions has been rekindled in recent years by the innovative work by Sridhar and co-workers[32−34] and Spiegelberg and McKinley[35,36] in measuring the properties of these liquids in filament stretching devices. The success of these devices has, in turn, spawned a new sequence of theoretical studies.[37−41] Nonetheless, there is still a wide gap between the states-of-the-art of experimental study of the properties of dilute solutions in these strong flows and theoretical predictions of those properties.

All theoretical attempts to describe the behavior of flowing polymeric liquids suffer from the inherent need—imposed by the sheer size and complexity of the molecules—to invoke some type of simplifying model for the polymer molecules. Even under the simplifications allowed by classical mechanics and pairwise additive potentials, these systems are simply too large and complicated to study their dynamics *exactly* when they are undergoing flow. Therefore, we are always left in a theoretical study with perplexing questions as to what important molecular features may have been omitted when a particular model was invoked. With the possible exceptions of the simplest dumbbell models, most molecular models describe chain topology in what we hope to be an adequate manner. The most drastic of the assumptions imposed by the invocation of a model regard the forces (or, equivalently, the potentials) describing interactions between units on the same or different molecules.

Our purpose with this paper is examination of the role of several types of intramolecular interactions in determining the steady elongational flow properties of infinitely dilute polymer solutions. The restriction to steady flow is required in order to include detailed interactions, and even under the restriction of steady flow, we must resort to Monte Carlo simulations. The hope is that elucidation of the types of interactions that are necessary to describe steady flow will provide useful information for the (admittedly more important) task of modeling nonsteady elongational flows with perhaps more simple models. We begin with a description of the detailed model that we use and the simulation strategy employed. Then we present the predictions of the simulations for several conformational and rheological properties of the solution, and we conclude with a discussion of the roles of the different types of forces in predicting macroscopic behavior.

Molecular Model and Simulation Method

We model an infinitely dilute polymer solution with a united atom representation,[42] and we use the notation of Bird et al.[43] The model consists of a chain of N interaction sites connected linearly by $N - 1$ bonds. The chain configuration is described by a set of bond vectors $\boldsymbol{Q}^{N-1} = (\boldsymbol{Q}_1, \boldsymbol{Q}_2, ..., \boldsymbol{Q}_{N-1})$ where $\boldsymbol{Q}_i$ is the vector from site i to site $i + 1$. The chain is described by a configuration distribution function $\psi(\boldsymbol{Q}^{N-1},t)$, defined such that $\psi(\boldsymbol{Q}^{N-1},t)\, d\boldsymbol{Q}^{N-1}$ (where $d\boldsymbol{Q}^{N-1}$ denotes $d\boldsymbol{Q}_1\, d\boldsymbol{Q}_2 ... d\boldsymbol{Q}_{N-1}$) is the probability that bond 1 is within $d\boldsymbol{Q}_1$ of $\boldsymbol{Q}_1$, bond 2 is within $d\boldsymbol{Q}_2$ of $\boldsymbol{Q}_2$, and so on, at time t. This distribution function is governed by the diffusion

* To whom correspondence should be addressed.

10.1021/ma001357q CCC: $20.00
Published on Web 08/29/2001

equation (cf. eq 15.1-7 of Bird et al.[43])

$$\frac{\partial \psi}{\partial t} = -\sum_j \frac{\partial}{\partial \boldsymbol{Q}_j} \cdot \left[\boldsymbol{\kappa} \cdot \boldsymbol{Q}_j \psi - \frac{1}{\zeta} \sum_k A_{jk} \left(kT \frac{\partial \psi}{\partial \boldsymbol{Q}_k} + F_k^{(c)} \psi \right) \right] \quad (1)$$

where the A_{jk} are the elements of the Rouse matrix (defined with diagonal elements equal to 2, immediate off-diagonal elements equal to -1, and other elements equal to zero), kT is the Boltzmann constant multiplied by the absolute temperature, ζ is a friction (hydrodynamic drag) coefficient describing interactions between a site on the chain with the solvent, and $F_k^{(c)}$ represents all the intramolecular forces associated with connector $\boldsymbol{Q}_k$.

The united atom model that we examine incorporates potentials for bond stretching:

$$\phi_j^{\mathrm{str}} = -\frac{H Q_0^{\,2}}{2} \ln\left[1 - \left(\frac{Q_j - r_{\mathrm{eq}}}{Q_0} \right)^2 \right] \quad (2)$$

bond bending:

$$\phi_j^{\mathrm{bnd}} = \frac{1}{2} k_\theta (\theta_j - \theta_{\mathrm{eq}})^2 \quad (3)$$

bond angle torsion:

$$\phi_j^{\mathrm{tors}} = V_0 + \frac{1}{2} V_1 (1 + \cos \Phi_j) + \frac{1}{2} V_2 (1 - \cos 2\Phi_j) + \frac{1}{2} V_3 (1 + \cos 3\Phi_j) \quad (4)$$

and nonbonded interactions:

$$\phi_j^{\mathrm{LJ}} = 4\epsilon \left[\left(\frac{\sigma}{Q_j} \right)^{12} - \left(\frac{\sigma}{Q_j} \right)^{6} \right] \quad (5)$$

These potentials are the same as those used in the united-atom representation of Khare et al.[42] The stretching potential is similar to the *finitely extensible nonlinear elastic* (FENE) potential of Warner[44] (where H is the spring constant and Q_0 is the maximum length), but it also has the additional parameter, r_{eq}, that allows for stretching about a nonzero equilibrium bond length. Consequently, $Q_0 + r_{\mathrm{eq}}$ becomes the maximum bond length. The angle between bond vectors $\boldsymbol{Q}_i$ and $\boldsymbol{Q}_{i+1}$ is denoted by θ_i, and the bending potential is in the form of the so-called "θ expansion",[45] where θ_{eq} is the equilibrium bending angle and k_θ a bending constant. The expression for the torsion potential is a Fourier expansion of the potential in the torsion angle Φ_j with the Fourier coefficients V_i reflecting the barrier heights for rotation. The nonbonded potential uses the common Lennard-Jones 12−6 function where the first term, involving the distance to the inverse 12th power, represents the repulsive interactions and the second term, involving the inverse sixth power of the distance, represents the attractive van der Waals interaction. The repulsive term incorporates the important excluded-volume feature in the united-atom representation. We use the same parameter values in the potentials as Khare et al.[42] However, we set the Lennard-Jones parameters as $\epsilon/k = 47$ K and $\sigma = 0.75(Q_0 + r_{\mathrm{eq}})$. These are chosen to ensure that eq 5 incorporates excluded volume; that is, that it prevents the chain from passing through itself. Specific values for the parameters used are given in Table 1.

Table 1. Parameter Values Used in the United Atom Model[a]

bond stretching	$H = 96500$ K/Å^2
	$Q_0 = 1.572$ Å
	$0 \le r_{\mathrm{eq}} \le Q_0$
bond bending	$\theta_{\mathrm{eq}} = 114°$
	$k_\theta = 62500$ K/rad^2
bond angle torsion	$V_0 = 0$ K
	$V_1 = 355.03$ K
	$V_2 = -68.19$ K
	$V_3 = 701.32$ K
nonbonded	$\epsilon = 47$ K
	$\sigma = 0.75\ (r_{\mathrm{eq}} + Q_0)$

[a] The equilibrium length of a bond, r_{eq}, is varied through the dimensionless parameter s.

We now restrict our attention to steady homogeneous potential flows wherein the transpose of the velocity gradient $\boldsymbol{\kappa}$ is symmetric and constant. For these flows, it can be shown[43] that the solution of eq 1 is

$$\psi = \frac{1}{J} \exp\left[-\left(\frac{\phi}{kT} - \frac{\zeta}{2kT} \boldsymbol{\kappa} : \sum_{ij} C_{ij} \boldsymbol{Q}_i \boldsymbol{Q}_j \right) \right] \quad (6)$$

where ϕ is the total potential energy of the molecule, ζ is a hydrodynamic drag (friction) coefficient describing the interactions between the solvent and a site on the polymer molecule, the C_{ij} are the elements of the Kramers matrix (the inverse of the Rouse matrix), J is a constant chosen so that ψ is normalized to unity, and the summations extend over all of the bonds in a polymer molecule. The particular homogeneous potential flow that we consider is steady uniaxial elongational flow. For this flow $\boldsymbol{\kappa}$ is given by

$$\boldsymbol{\kappa} = \begin{bmatrix} -(1/2)\dot{\epsilon} & 0 & 0 \\ 0 & -(1/2)\dot{\epsilon} & 0 \\ 0 & 0 & \dot{\epsilon} \end{bmatrix} \quad (7)$$

where $\dot{\epsilon}$ is the constant elongation rate.

We use the distribution function given by eq 6 to calculate average properties of the solution beginning with the elongational viscosity. The polymer contribution to the stress tensor is[43]

$$\boldsymbol{\tau}_{\mathrm{p}} = (N-1) nkT \boldsymbol{\delta} + n \sum_{\nu=1}^{N} \langle \boldsymbol{R}_\nu \boldsymbol{F}_\nu^{(\phi)} \rangle \quad (8)$$

where n is the number density of polymer chains, $\boldsymbol{\delta}$ is the second-order unit tensor, $\boldsymbol{F}_\nu^{(\phi)}$ is the total force on site ν from the potentials given by eqs 2−5, and $\boldsymbol{R}_\nu$ is the location of site ν relative to the center of mass of the molecule. The dimensionless elongational viscosity is computed from this using the definition

$$\frac{\bar{\eta} - 3\eta_{\mathrm{s}}}{nkT\lambda} = \frac{\tau_{\mathrm{p},xx} - \tau_{\mathrm{p},zz}}{nkT\lambda\dot{\epsilon}} \quad (9)$$

where η_{s} is the solvent viscosity. For a time constant we somewhat arbitrarily choose $\lambda = \zeta Q_0^2/12kT$. It is not possible to determine the appropriate time constant for these chains without performing some type of transient simulation. The harmonic oscillator time constant, λ_H based on the spring coefficient, H, is not appropriate, because the springs here represent very stiff bonds. We simply adopt the fundamental time constant for a rigid rotator of length Q_0, which is several orders of magnitude larger than λ_H.

In addition, we calculate conformational properties for the chain including the mean-square end-to-end distance for the chain:

$$\langle r^2 \rangle = (\sum_{ij} \langle \boldsymbol{Q}_i \cdot \boldsymbol{Q}_j \rangle) \tag{10}$$

The average moment of inertia of the chain about the principal flow axis[25] (the *z*-axis) defined by

$$\langle I_{zz} \rangle = m \sum_{ij} C_{ij} \langle Q_{ix} Q_{jx} + Q_{iy} Q_{jy} \rangle \tag{11}$$

(where *m* is the mass associated with a site on the chain) is of interest, because it indicates how well the chains are aligned in the flow direction. We normalize the values computed from eq 11 by $\langle I_{zz} \rangle_{eq}$, the average moment of inertia at equilibrium (no flow), so that $\langle I_{zz} \rangle / \langle I_{zz} \rangle_{eq}$ is equal to unity when the chains are, on average, spherically symmetric (in the no-flow, equilibrium state). This ratio is equal to zero when the chains are perfectly aligned with the flow axis.

The averages in eqs 9−11 can be calculated directly from eq 6 in principle, but the integrals are extremely difficult to evaluate analytically. In addition, standard numerical integration methods are not suitable, because of the large dimensionality of the integrals. However, the averages are amenable to Monte Carlo integration—a method that randomly samples an integrand and uses the values to form an accumulator. As the number of samples approaches infinity, the average of the accumulator tends to the value of the integral.

The Metropolis algorithm[46] provides an efficient way to sample the configuration space for carrying out Monte Carlo integration. In a typical Metropolis scheme, one of the sites in the chain is randomly displaced. This changes the potential energy of the configuration. If the energy change is negative, the move is accepted. If the energy change is positive, then the move is accepted depending on the magnitude of the change relative to a suitably chosen random number. Large energy configurations are improbable and do not contribute significantly to the averages, and the Metropolis algorithm is efficient because it favors those configurations that contribute significantly to the averages. The sampling process is repeated many times for all the beads in the chain to obtain good approximations for the averages.

In this work, we implement the *continuum configurational bias* approach used by de Pablo et al.[47]—a modified Metropolis technique. A site along the chain is selected at random, but rather than moving just that site, the part of the chain from that site to one of the ends is moved. This can be visualized as regrowing the chain segment by segment from a randomly chosen site. The motivation for using this approach is twofold. First, moving a larger part of the chain at each step enables the moves to be made over a bigger region of the chain configuration space. Second, the chain can easily come out of any "excluded-volume knots" caused by the nonbonded potential. This is essential when the averages are being computed for very low elongation rates. An added advantage of the technique is that reliable averages are obtained in a smaller number of simulation steps when compared to the regular Metropolis method. The computational disadvantage of a configurational bias approach arises from the need to remove the effect of the bias on the averages that are computed; we use the method described by de Pablo et al.[47] for removing this bias. For our simulations, the number of samplings was of the order of 10^7. The initial chain configurations were chosen randomly, and the system was allowed to "equilibrate" for a long period (about 10^6 steps) before we start calculating averages.

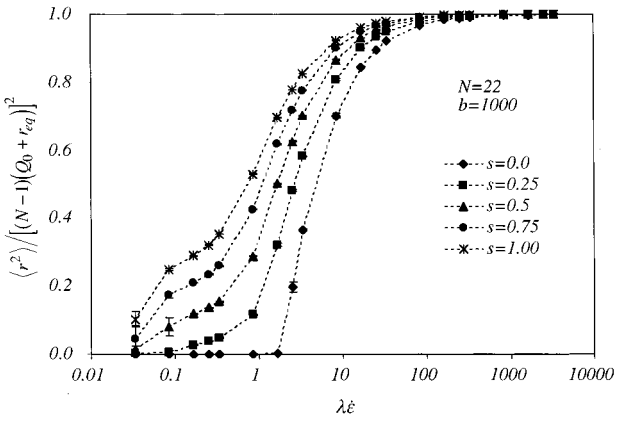

Figure 1. Mean-squared end-to-end distance for chains that incorporate only bond stretching potentials. The curves are for different values of the equilibrium bond length, and the dashed lines are included just to aid the eye.

Results

We present results in terms of two dimensionless parameters *s* and *b*. The parameter *s* is the ratio of the equilibrium to maximum bond length (r_{eq}/Q_0). It is a measure of how much the bond length is allowed to fluctuate about the equilibrium value. When *s* is zero, the stretching potential reduces to the Warner FENE potential.[44] The parameter *b* is equal to HQ_0^2/kT and reflects the finite extensibility of the bonds. In the limit of infinite *b* we recover the Rouse chain when the other potentials are absent. Errors are estimated using standard methods,[46] and error bars are shown on the figures. It must be noted that the error bars for the elongational viscosity plots are relatively larger at low elongation rates when compared to those for the mean-squared end-to-end distance and *z* moment of inertia. This is partly because the elongation viscosity expression includes the elongation rate in the denominator. When error bars are not shown, the errors are smaller than the symbols marking the data points. It is also important to note that the simulation results presented here are for relatively short chains. It is not our intent to elucidate the scaling behavior with molecular weight of the properties calculated.

We begin by presenting results for the model without bending, torsion, or nonbonded potentials, that is, for a freely rotating, phantom chain with bond stretching governed by eq 2. When *s* is equal to zero, these results reduce to those of Kobe and Wiest[31] for FENE chains. Figure 1 shows the predictions for the mean-squared end-to-end distance for different values of *s*, and Figure 2 shows the corresponding values for $\langle I_{zz} \rangle / \langle I_{zz} \rangle_{eq}$. Inclusion of nonzero bond length decreases the elongation rate at which the chains adopt stretched, linear conformations. This results in a decrease in the elongation rate at which the elongational viscosity increases dramatically to its infinite elongation rate asymptote as seen in Figure 3. Figures 4−6 are the analogues of Figures 1−3 but for variation in the length (number of sites) of the chain. Variation in *N* for the model with nonzero *s* has nearly the same effect as it does for the model with $s = 0$.[31]

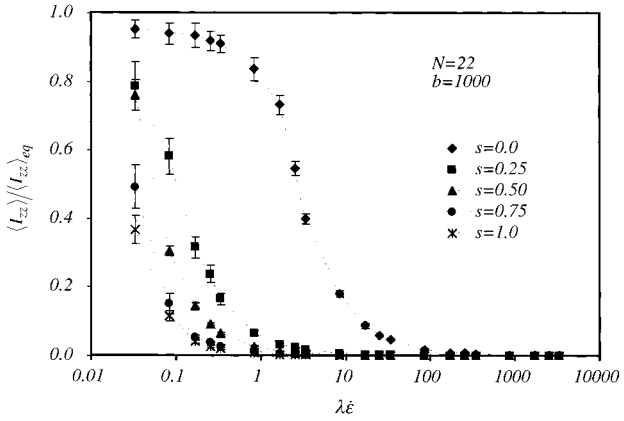

Figure 2. Normalized average moment of inertia about the principal flow axis for chains that incorporate only bond stretching potentials. The curves are for different values of the equilibrium bond length, and the ratio approaches zero when the chains are (on average) perfectly aligned in the flow direction.

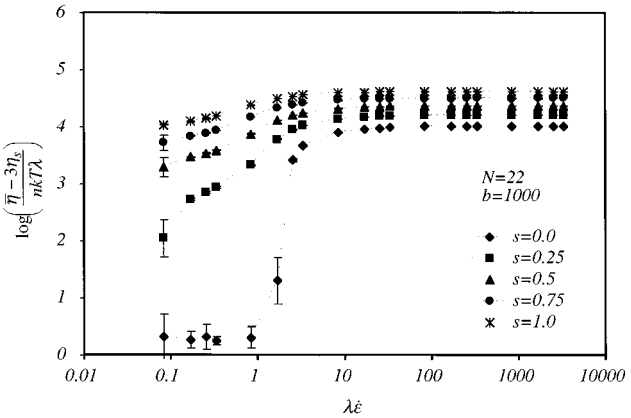

Figure 3. Dimensionless polymer contribution to the elongational viscosity predictions for chains that incorporate only bond stretching potentials. The curves are for different values of the equilibrium bond length.

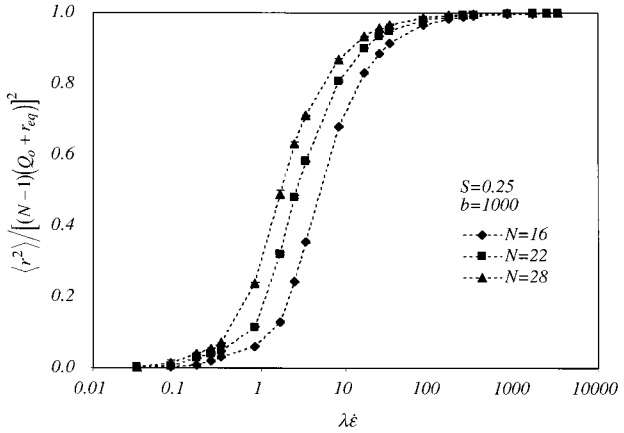

Figure 4. Mean-squared end-to-end distance for chains that incorporate only bond stretching potentials. The curves are for different chain lengths (number of sites).

Now we turn our attention to the model including all of the potentials in eqs 2−5. Figure 7 shows the mean-squared end-to-end distance for chains of varying number of sites. The large elongation rate behavior of these predictions is similar to that shown in Figure 1, but there are qualitative differences at low to intermediate elongation rates. Figure 8 gives the predictions for the normalized average moment of inertia about the principal flow axis for chains with varying number of sites, and Figure 9 gives the predictions of the elongational viscosity. Again, the behavior at large elongation rates is qualitatively similar to that shown in Figures 2 and 3, but there are significant differences at low to intermediate elongation rates.

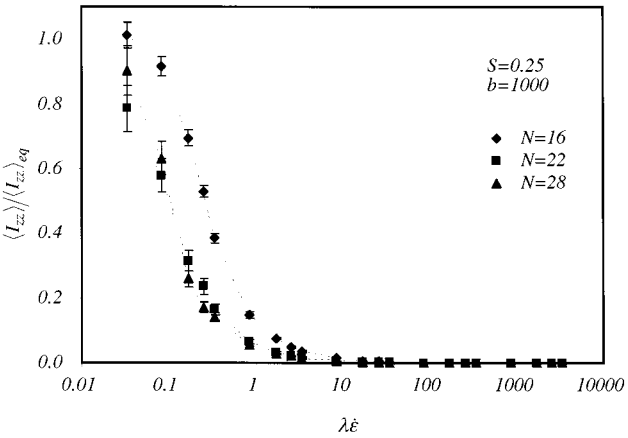

Figure 5. Normalized average moment of inertia about the principal flow axis for chains that incorporate only bond stretching potentials. The curves are for different chain lengths (number of sites).

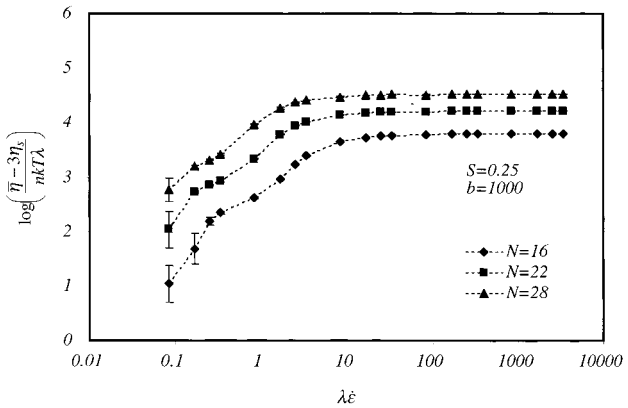

Figure 6. Dimensionless polymer contribution to the elongational viscosity for chains that incorporate only bond stretching potentials. The curves are for different chain lengths (number of sites), and the curves just connect the points.

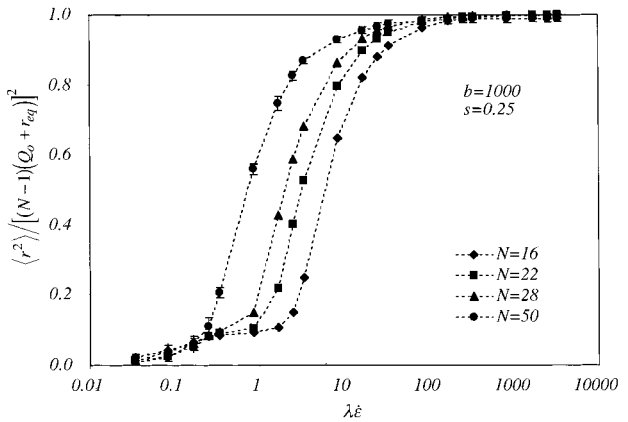

Figure 7. Mean-squared end-to-end distance predictions for the full united atom model. The curves are for different chain lengths (number of sites).

To explore the differences between the results shown in Figures 1−3 and those shown in Figures 7−9, we examine models that include various combinations of

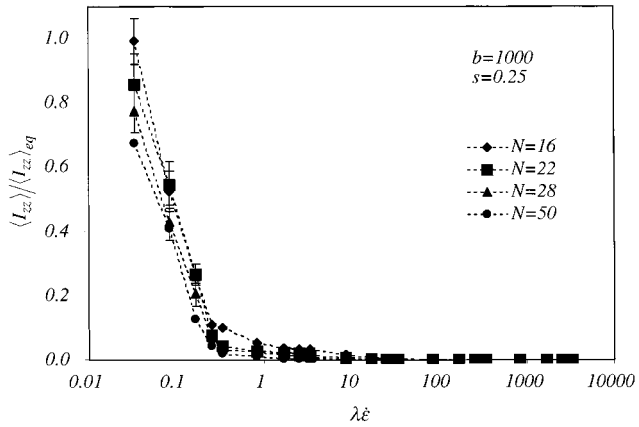

Figure 8. Normalized average moment of inertia about the principal flow axis for the full united atom model. The curves are for different chain lengths (number of sites).

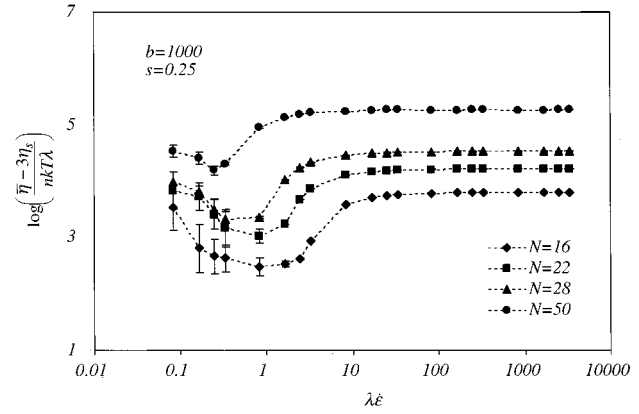

Figure 9. Dimensionless polymer contribution to the elongational viscosity predictions for the full united atom model. The curves are for different chain lengths (number of sites).

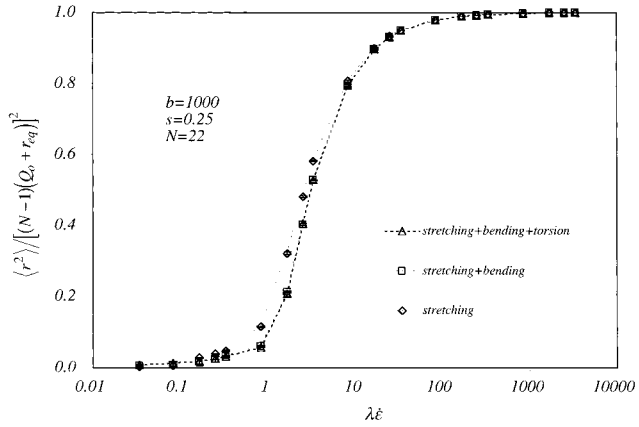

Figure 10. Mean-squared end-to-end distance predictions for models incorporating the indicated bond potentials and no nonbonded interactions.

the potentials in eqs 2−5. Figures 10, 11, and 12 give the mean-squared end-to-end distance, average moment of inertia about the principal flow axis, and polymer contribution to the elongational viscosity, respectively, for models that incorporate various contributions to the potential from eqs 2−4 but do not include nonbonded interactions. For the geometric properties ($\langle r^2\rangle$ and $\langle I_{zz}\rangle$), bond bending makes a significant contribution over bond stretching, but the torsional potential does not. Torsion does play a slightly larger role in the elongational viscosity at low to moderate elongation rates. In Figures

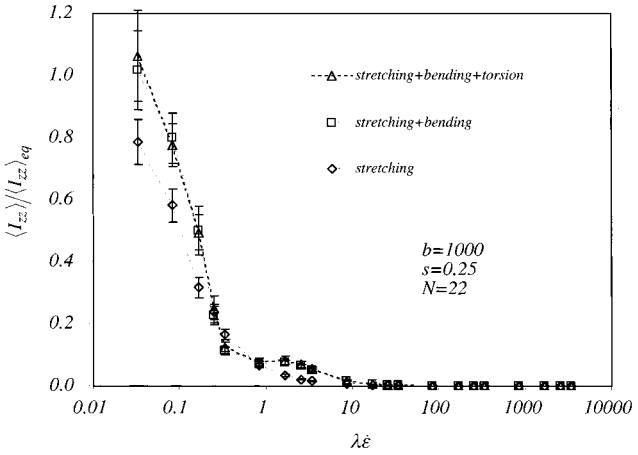

Figure 11. Normalized average moment of inertia about the principal flow axis for models incorporating the indicated bonded interactions and no nonbonded interactions.

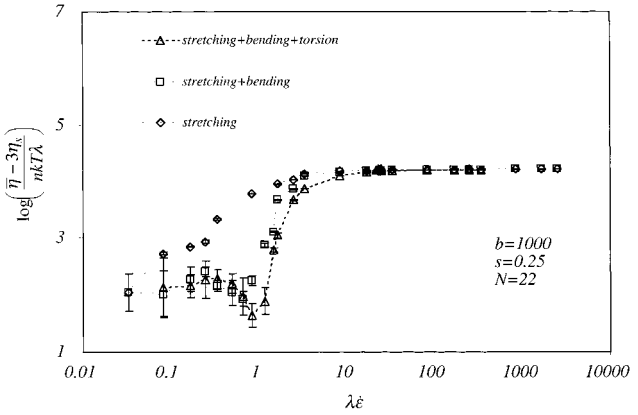

Figure 12. Dimensionless polymer contribution to the elongational viscosity for chains that incorporate the indicated bond interactions and no nonbonded interactions.

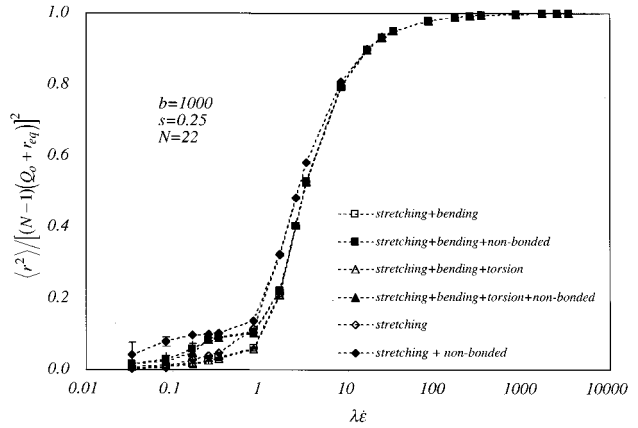

Figure 13. Mean-squared end-to-end distance predictions for models incorporating the indicated bonded and nonbonded interactions. Solid symbols are for models that include nonbonded interactions, and open symbols are for those that do not.

13, 14, and 15 we show the effects on the mean-squared end-to-end distance, average moment of inertia about the principal flow axis, and polymer contribution to the elongational viscosity of nonbonded interactions (eq 5) between the chain sites. The nonbonded interactions have very little effect on any of the predictions at large elongation rates, but they have significant effects at low to moderate elongation rates.

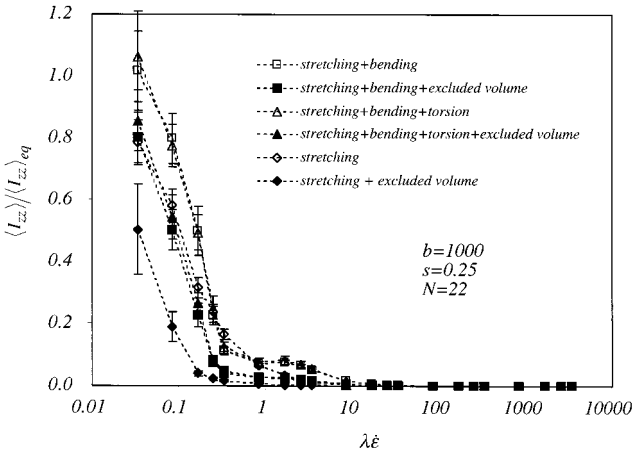

Figure 14. Normalized average moment of inertia about the principal flow axis for models incorporating the indicated bonded and nonbonded interactions. Solid symbols are for models that include nonbonded interactions, and open symbols are for those that do not.

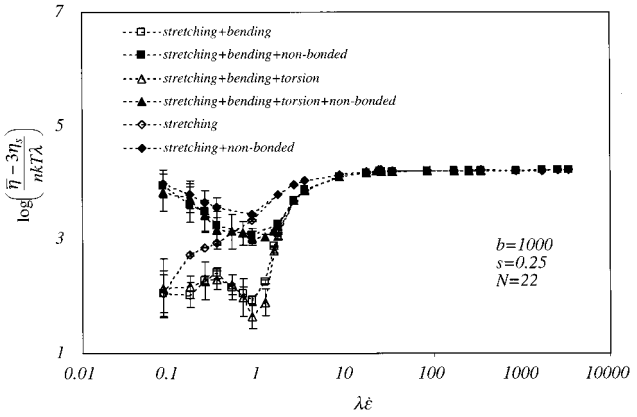

Figure 15. Dimensionless polymer contribution to the elongational viscosity for models incorporating the indicated bonded and nonbonded interactions. Solid symbols are for models that include nonbonded interactions, and open symbols are for those that do not.

Discussion

It is clear from the results presented above that some intramolecular potentials play a much more important role than others in steady uniaxial elongational flow. Figures 1−3 demonstrate that, other than in determining the elongation rate at which the chains change from a primarily coiled to a primarily stretched configuration in the flow, the detailed shape of the bond potential (within the general framework of a finitely extensible potential) has only a quantitative effect. Nonzero values of the parameter *s* add a compressive component to the bond stretching potential and result in the bonds being, on average, longer (even at equilibrium). This results in the subunits of the molecule being more exposed to the flow, so that weaker elongational flows can deform the chains more substantially. The same effect is observed in Figures 4−6 for increasing the length of the chain. Weaker elongational flows can more easily deform long chains that have more interaction sites. However, Figure 5 demonstrates that the average shape of the chain does not change much for chains of 22 or more sites.

Figures 4, 5, and 6 should be compared with Figures 7, 8, and 9, respectively, to examine the combined effect of the potentials for bond torsion, bond bending, and nonbonded interactions on the predicted behavior. Comparison of Figures 5 and 8 shows that the additional potentials result in $\langle I_{zz} \rangle$ approaching zero more abruptly and at a lower elongation rate ($\lambda\dot{\epsilon} \sim 0.2$). This can be interpreted as the potentials causing the chains to be aligned in the principal flow direction, on average, at a lower elongation rate. Furthermore, the deformation of the chains away from their spherically symmetric, equilibrium configurations to aligned configurations is more sensitive to elongation rate when the additional forces are included. However, comparison of Figures 4 and 7 shows that this picture is overly simplistic. Inclusion of the additional potentials results in a relatively low "plateau" in $\langle r^2 \rangle$ at elongation rates where $\langle I_{zz} \rangle$ is nearly zero (i.e., in the region $0.2 \leq \lambda\dot{\epsilon} \leq 2$ in Figure 7). This indicates that, whereas the mass of the molecule is primarily along the principal flow axis (Figure 8), the chains are not stretched appreciably. This is consistent with the chains being in folded-but-aligned conformations at these elongation rates.[25] Possible reasons for this are considered below.

The most striking differences that are induced by inclusion of the additional potentials occur in the predictions of the elongational viscosity (Figure 9). Whereas the model with only bond stretching potentials predicts that the elongational viscosity always increases with increasing elongation rate until the infinite elongation rate asymptote is reached, the additional potentials result in much more interesting predictions. Considering the behavior as $\lambda\dot{\epsilon}$ decreases from high elongation rates (where the infinite elongation rate asymptote is a function of only N and b),[26] we see that the elongational viscosity first decreases more steeply as a result of the additional potentials, but it then reaches a plateau and begins to increase for even smaller elongation rates. This results in a minimum value in $\bar{\eta}$ at a moderate elongation rate. Similar behavior has been predicted by Fetsko and Cummings.[48]

To understand the effects of the intramolecular potentials on the geometric predictions, as well as the unusual predictions for $\bar{\eta}$, we now consider the predictions of models containing only subsets of the potentials given in eqs 2−5. First we consider the effects of the bonded potentials, that is, omitting the nonbonded potential of eq 5. These results are in Figures 10−12. In Figure 10, we see that, in the absence of nonbonded interactions, addition of a bending potential to the stretching potential has a small effect on the mean-square end-to-end distance for the chains, but addition of the torsional potential has practically no effect on this geometric quantity. For the average moment of inertia in Figure 11 we see that, again, the torsional potential has only a minimal effect, but the bending potential has a somewhat larger effect with the chains remaining more spheroidal until larger elongation rates. The flow has to be stronger in order to overcome the resistance to alignment caused by the bending potentials. In addition, we see that the bending potentials give rise to the small, nonzero plateau in $\langle I_{zz} \rangle$. This plateau occurs just below the elongation rate at which the mean-square end-to-end distance shows its abrupt increase, so we can surmise that it is a consequence of the bending potentials causing the flow to have to be stronger in order to deform the chains out of their folded-but-aligned conformations into stretched conformations. That is, the bending potentials cause the chains to be harder to deform out of their folded-but-aligned conformations.

We see in Figure 12 that part of the unusual behavior of $\bar{\eta}$ that we observe in Figure 9 is a consequence of the bending potentials. Namely, the plateau in $\bar{\eta}$ and the abrupt increase appear to be a consequence of these potentials (and to be effected only minimally by the torsional potentials). Furthermore, this increase occurs at the end of the plateau discussed in the previous paragraph. The elongational viscosity is low for the folded conformations but is higher for the stretched conformations. As with $\langle r^2 \rangle$ and $\langle I_{zz} \rangle$, the torsional potentials have only a small effect on $\bar{\eta}$.

We now turn our attention to the roles played by nonbonded interactions (Figures 13−15). In each of these figures, closed symbols are used for results that include nonbonded interactions and open symbols are used for results that exclude nonbonded interactions. In Figure 13 we see that nonbonded interactions have no effect on $\langle r^2 \rangle$ at large elongation rates; the chains are stretched. However, at low elongation rates the nonbonded interactions cause $\langle r^2 \rangle$ to be larger as a result of excluded-volume effects. In Figure 14 we note that the nonbonded interactions result in the chain being deformed away from its spherical equilibrium conformation at somewhat lower elongation rates. The folded-but-aligned plateau[25] in $\langle I_{zz} \rangle$ is still present at intermediate elongation rates, but it is suppressed. As a result of the excluded volume, the chains are more extended coming into the plateau region, and the chains are somewhat more aligned and stretched than folded. Again, at high elongation rates the nonbonded interactions have little effect; the chains are stretched and aligned.

Figure 15 indicates that the existence of a minimum value in $\bar{\eta}$ at moderate elongation rates is a consequence of nonbonded interactions, presumably excluded volume. Fetsko and Cummings[48] observed a similar effect, but they incorporated excluded volume by way of modifications to the stretching potential and associated the increased elongational viscosity at low elongation rates with a reduction in the maximum possible bond extension. However, Figure 15 demonstrates that there must be some additional effect. It seems plausible that the increase is due in part to the larger chain size (i.e., larger $\langle r^2 \rangle$) at low elongation rates. Figure 14 indicates that the chains are less spherical at low elongation rates when the nonbonded interactions are included, and this will cause an increase in $\bar{\eta}$. Furthermore, the nonbonded interactions should hamper chain rearrangements in the coiled and nearly coiled states. This would result in increased dissipation of energy and, hence, a larger elongational viscosity. The chains are less exposed to the flow in the folded-but-aligned conformations at intermediate elongation rates, so the dissipation and elongational viscosity are lower. In the fully stretched conformations at large elongation rates, the dissipation and elongational viscosity are again large.

In summary, we can conclude that bending and nonbonded interactions play important roles in the behavior of dilute polymer solutions undergoing steady uniaxial elongational flow. On the other hand, torsional potentials are less important, having only smaller, quantitative effects. Of course, these conclusions are limited by the chain lengths we considered (up to 50 sites).

Acknowledgment. The authors gratefully acknowledge financial support provided by the National Science Foundation through the Materials Science Research and Engineering Center at the University of Alabama (DMR-9809423) and by the SOMED program of the University of Alabama. In addition, they acknowledge computational resources provided by the Alabama Institute for Manufacturing Excellence.

References and Notes

(1) Pope, D. P.; Keller, A. *Colloid Polym. Sci.* **1977**, *255*, 633−643.
(2) Fuller, G. G.; Leal, L. G. *Rheol. Acta* **1980**, *19*, 580−600.
(3) Dunlap, P. N.; Leal, L. G. *J. Non-Newtonian Fluid Mech.* **1987**, *23*, 5−48.
(4) Miles, M. J.; Keller, A. *Polymer* **1980**, *21*, 1295−1298.
(5) Lyazid, A.; Scrivener, O.; Teitgen, R. In *Rheology*; Astarita, G., Marrucci, G., Nicolais, L., Eds.; Plenum Press: New York, 1980; Vol. 2, pp 141−148.
(6) Gardener, K.; Pike, E. P.; Miles, M. J.; Keller, A.; Tanaka, K. *Polymer* **1982**, *23*, 1435−1442.
(7) Odell, J. A.; Keller, A.; Miles, M. J. *Polymer* **1985**, *26*, 1219−1226.
(8) Odell, J. A.; Keller, A. *J. Polym. Sci., Polym. Phys. Ed.* **1986**, *24*, 1889−1916.
(9) Farinato, R. S. *Polymer* **1988**, *29*, 160−167.
(10) Chauveteau, G.; Moan, M.; Magueur, A. *J. Non-Newtonian Fluid Mech.* **1984**, *16*, 315−327.
(11) James, D. F.; McLean, B. D.; Saringer, J. H. *J. Rheol.* **1987**, *31*, 453−481.
(12) Wunderlich, A. M.; James, D. F. *Rheol. Acta* **1987**, *26*, 522−531.
(13) Mackley, M. R.; Keller, A. *Philos. Trans. R. Soc. (London)* **1975**, *278*, 29−66.
(14) Pope, D. P.; Keller, A. *Colloid Polym. Sci.* **1978**, *256*, 751−756.
(15) Farrell, C. J.; Keller, A.; Miles, M. J.; Pope, D. P. *Polymer* **1980**, *21*, 1292−1294.
(16) Peiffer, D. G.; Kim, M. W.; Lundberg, R. D. *Polymer* **1986**, *27*, 493−502.
(17) Peiffer, D. G.; Kim, M. W.; Schulz, D. N. *J. Polym. Sci., Polym. Phys. Ed.* **1987**, *25*, 1615−1628.
(18) Fuller, G. G.; Cathey, C. A.; Hubbard, B.; Zebrowski, B. E. *J. Rheol.* **1987**, *31*, 235−249.
(19) Chow, A.; Keller, A.; Muller, A. J.; Odell, J. A. *Macromolecules* **1988**, *21*, 250−256.
(20) Odell, J. A.; Muller, A. J.; Keller, A. *Polymer* **1988**, *29*, 1179−1190.
(21) Cathey, C. A.; Fuller, G. G. *J. Non-Newtonian Fluid Mech.* **1990**, *34*, 63−88.
(22) Odell, J. A.; Muller, A. J.; Narh, K. A.; Keller, A. *Macromolecules* **1990**, *23*, 3092−3103.
(23) de Gennes, P. G. *J. Chem. Phys.* **1974**, *60*, 5030.
(24) Fan, X.-J.; Bird, R. B.; Renardy, M. *J. Non-Newtonian Fluid Mech.* **1985**, *18*, 255.
(25) Wiest, J. M.; Wedgewood, L. E.; Bird, R. B. *J. Chem. Phys.* **1989**, *90*, 587−594.
(26) Wiest, J. M.; Tanner, R. I. *J. Rheol.* **1989**, *33*, 281−316.
(27) Wedgewood, L. E.; Öttinger, H. C. *J. Non-Newtonian Fluid Mech.* **1988**, *27*, 245−264.
(28) Acierno, D.; Titomanlio, G.; Marrucci, G. *J. Polym. Sci., Polym. Phys. Ed.* **1974**, *12*, 2177−2187.
(29) Rallison, J. M.; Hinch, E. J. *J. Non-Newtonian Fluid Mech.* **1988**, *29*, 37−55.
(30) Liu, T. W. *J. Chem. Phys.* **1990**, *90*, 5826−5842.
(31) Kobe, J. M.; Wiest, J. M. *J. Rheol.* **1993**, *37*, 947−960.
(32) Tirtaatmadja, V.; Sridhar, T. *J. Rheol.* **1993**, *37*, 1081−1102.
(33) Tirtaatmadja, V.; Sridhar, T. *J. Rheol.* **1995**, *39*, 1133−1160.
(34) Orr, N. V.; Sridhar, T. *J. Non-Newtonian Fluid Mech.* **1996**, *67*, 77−103.
(35) Spiegelberg, S. H.; McKinley, G. H. In *Proceedings of the XIIth International Congress on Rheology*; Ait-Kadi, A., Dealy, J. M., James, D. F., Williams, M. C., Eds.; Laval University Press: Quebec City, 1996.
(36) Spiegelberg, S. H.; McKinley, G. H. *J. Non-Newtonian Fluid Mech.* **1996**, *67*, 49−76.
(37) Doyle, P. S.; Shaqfeh, E. S. G.; McKinley, G. H.; Spiegelberg, S. H. *J. Non-Newtonian Fluid Mech.* **1998**, *76*, 81−112.
(38) Wiest, J. M. *Polymer* **1999**, *40*, 1917−1922.
(39) Wiest, J. M. *J. Chem. Phys.* **1999**, *111*, 5205−5211.
(40) Li, L.; Larson, R. G.; Sridhar, T. *J. Rheol.* **2000**, *44*, 291−321.

(41) Doyle, P. S.; Shaqfeh, E. S. G. *J. Non-Newtonian Fluid Mech.* **1998**, *76*, 43−78.
(42) Khare, R.; de Pablo, J. J.; Yethiraj, A. *J. Chem. Phys.* **1997**, *107*, 6956−6964.
(43) Bird, R. B.; Curtiss, C. F.; Armstrong, R. C.; Hassager, O. *Dynamics of Polymeric Liquids;* Wiley-Interscience: New York, 1987; Vol. 2.
(44) Warner, H. R., Jr. *Ind. Eng. Chem. Fundam.* **1972**, *11*, 379−381.
(45) Colburn, E. A. *Computer Simulation of Polymers*; Longman Press: London, 1994.
(46) Allen, M. P.; Tildesley, D. J. *Computer Simulation of Liquids*; Clarendon Press: Oxford, 1987.
(47) de Pablo, J. J.; Laso, M.; Suter, U. W. *ACS Polym. Prepr.* **1992**, *33*, 594−595.
(48) Fetsko, S. W.; Cummings, P. T. *J. Rheol.* **1995**, *39*, 285−299.

MA001357Q